Editors' Suggestion

Optical Modulation of Electron Beams in Free Space

F. Javier García de Abajo[1,2,*] and Andrea Konečná[1]

[1]ICFO-Institut de Ciencies Fotoniques, The Barcelona Institute of Science and Technology, 08860 Castelldefels (Barcelona), Spain
[2]ICREA-Institució Catalana de Recerca i Estudis Avançats, Passeig Lluís Companys 23, 08010 Barcelona, Spain

(Received 7 November 2020; accepted 16 February 2021; published 22 March 2021)

We exploit free-space interactions between electron beams and tailored light fields to imprint on-demand phase profiles on the electron wave functions. Through rigorous semiclassical theory involving a quantum description of the electrons, we show that monochromatic optical fields focused in vacuum can be used to correct electron beam aberrations and produce selected focal shapes. Stimulated elastic Compton scattering is exploited to imprint the required electron phase, which is proportional to the integral of the optical field intensity along the electron path and depends on the transverse beam position. The required light intensities are attainable in currently available ultrafast electron microscope setups, thus opening the field of free-space optical manipulation of electron beams.

DOI: 10.1103/PhysRevLett.126.123901

Electron microscopy has experienced impressive advances over the last decades thanks to the design of sophisticated magnetostatic and electrostatic lenses that reduce electron optics aberrations [1–3] and are capable of focusing electron beams (e-beams) with subångstrom precision [4,5]. In addition, the availability of more selective monochromators [6] enables the exploration of sample excitations down to the midinfrared regime [7–10]. Such accurate control over e-beam shape and energy is crucial for atomic-scale imaging and spectroscopy [1–10].

The focused e-beam profile ultimately depends on the phase acquired by the electron along its passage through the microscope column. By imprinting an on-demand transverse phase profile on the electron wave function, one can shape the e-beam density distribution at the specimen, creating, for example, multifocal configurations to study atomic structures and delocalized optical modes through elastic [11] and inelastic [12] holography, respectively. Additionally, temporal control over the phase and the resulting focal shape in the subpicosecond domain would grant us access into structural and excitation dynamics, suggesting the use of coherent control techniques [13] to optimize the phase for the desired application.

Besides electron optics lenses, several physical elements have been demonstrated to control transverse e-beam shaping. In particular, biprisms based on biased wires provide a dramatic example of laterally varying phase imprinting that is commonly used for e-beam splitting in electron holography [11], along with applications such as symmetry-selected plasmon excitation in metallic nanowires [14]. In a related context, vortex e-beams have been realized using a magnetic pseudomonopole [15]. Recently, plates with individually biased perforations have been developed to enable position-selective control over the electric Aharonov-Bohm phase stamped on the electron wave function [16], while passive carved plates have been employed as amplitude filters to produce highly chiral electron vortices [17–19] and aberration correctors [20,21].

The electron phase can also be modified by the ponderomotive force associated with the interaction between e-beams and optical fields. In particular, periodic light standing waves were predicted to produce electron diffraction [22], which was eventually observed in a challenging experiment [23–25] that had to circumvent the weak free-space electron-photon coupling associated with an energy-momentum mismatch [26]. Such a mismatch forbids single photon emission or absorption processes by free electrons, consequently limiting electron-light coupling to second-order interactions that concatenate an even number of virtual photon events. This type of interaction has been recently exploited to produce attosecond free-electron pulses [27,28].

Interestingly, the presence of material structures introduces scattered optical fields that can supply momentum and break the mismatch, thus enabling the occurrance of real photon processes [26] used, for example, in laser-driven electron accelerators [29,30]. Because the strength of scattered fields reflects the nanoscale optical response of the materials involved, this phenomenon was speculated to enable electron energy-gain spectroscopy as a way to dramatically improve spectral resolution in electron microscopes [31–33], as later corroborated in experiment [34]. By synchronizing the arrival of electron and light pulses at the sample, photon-induced near-field electron microscopy (PINEM) was demonstrated to exert temporal control over the electron wave function along the beam direction [35–58]. Additionally, modulation of the transverse wave function can be achieved in PINEM by laterally shaping the employed light [59], which results in the transfer of linear [49,60] and angular [53,61] momentum between photons and electrons.

Recently, we have proposed to use PINEM to imprint on-demand transverse e-beam phase profiles [62], thus relying on ultrafast e-beam shaping as an alternative approach to aberration correction. This method enables fast active control over the modulated e-beam at the expense of retaining only $\sim 1/3$ of monochromatic electrons and potentially introducing decoherence through inelastic interactions with the light scatterer. An approach to phase molding in which no materials are involved and the electron energy is preserved would then be desirable.

In this Letter, we propose an optical free-space electron modulator (OFEM) in which a phase profile is imprinted on the transverse electron wave function by means of the stimulated elastic Compton scattering associated with the A^2 term in the light-electron coupling Hamiltonian. The absence of material structures prevents electron decoherence and enables the use of high light intensities, as required to activate ponderomotive forces. We present a simple, yet rigorous semiclassical theory that supports applications of OFEM in aberration correction and transverse e-beam shaping. While optical e-beam phase stamping has been demonstrated in tour-de-force experiments using continuous-wave lasers [63–65], we envision pulsed illumination as a more feasible route to implement an OFEM, exploiting recent advances in ultrafast electron transmission microscopes (UTEMs), particularly in systems that incorporate light injection with a high numerical aperture [52] for diffraction-limited patterning of the optical field.

Free-space optical phase imprinting.—We study the free-space interaction between an e-beam and a light field represented by its vector potential $\mathbf{A}(\mathbf{r},t)$, working in a gauge in which the electric potential vanishes. With the e-beam propagation direction taken along z, it is convenient to write the electron wave function as $\psi(\mathbf{r},t) = \mathrm{e}^{iq_0 z - iE_0 t/\hbar}\phi(\mathbf{r},t)$, where we separate the slowly varying envelope $\phi(\mathbf{r},t)$ from the fast oscillations imposed by the central wave vector q_0 and energy E_0. Under the typical conditions met in electron microscopes, and assuming that interaction with light only produces small variations in the electron energy compared to E_0, we can adopt the nonrecoil approximation to reduce the Dirac equation in the minimal coupling scheme to an effective Schrödinger equation (see Sec. S1 in the Supplemental Material (SM) [66]),

$$(\partial_t + \mathbf{v}\cdot\nabla)\phi(\mathbf{r},t) = \frac{-i}{\hbar}\mathcal{H}'(\mathbf{r},t)\phi(\mathbf{r},t),$$

where

$$\mathcal{H}' = \frac{e}{c}\mathbf{v}\cdot\mathbf{A} + \frac{e^2}{2m_e c^2\gamma}\left(A_x^2 + A_y^2 + \frac{1}{\gamma^2}A_z^2\right) \qquad (1)$$

is the interaction Hamiltonian, $\mathbf{v} = v\hat{\mathbf{z}}$ is the electron velocity, and $\gamma = 1/\sqrt{1 - v^2/c^2}$ introduces relativistic corrections to the A^2 term. This equation admits the analytical solution

$$\phi(\mathbf{r},t) = \phi_0(\mathbf{r} - \mathbf{v}t)\exp\left[\frac{-i}{\hbar}\int_{-\infty}^{t} dt'\mathcal{H}'(\mathbf{r} - \mathbf{v}t + \mathbf{v}t', t')\right],$$

where $\phi_0(\mathbf{r} - \mathbf{v}t)$ is the incident electron wave function.

We consider that the light field acts on the electron over a sufficiently short path length L as to neglect any transverse variation in its wave function during the interaction (e.g., $L \lesssim D/\theta_e \sim 1$ mm for an e-beam diameter $D \sim 1$ μm and a divergence angle $\theta_e \sim 1$ mrad). We also note that the $\mathbf{v}\cdot\mathbf{A}$ term in Eq. (1) does not contribute to the final electron state because it represents real photon absorption or emission events, which are kinematically forbidden (see Sec. S2 in the SM [66]). Likewise, following a similar argument, under monochromatic illumination with light of frequency ω, the time-varying components in A^2 ($\propto \mathrm{e}^{\pm 2i\omega t}$), which describe two-photon emission or absorption, also produce vanishing contributions. The remaining terms $\propto \mathrm{e}^{\pm i\omega t \mp i\omega t}$ represent stimulated elastic Compton scattering, a second-order process that combines virtual absorption and emission of photons, amplified by the large population of their initial and final states. An alternative description of this effect is provided by the ponderomotive force acting on a classical point-charge electron and giving rise to diffraction in the resulting effective potential [25]. As we are interested in imprinting a phase on the electron wave function without altering its energy, we consider spectrally narrow external illumination that can be effectively regarded as monochromatic, such as that produced by laser pulses of much longer duration than the electron pulse. Writing the light vector potential as $\mathbf{A}(\mathbf{r},t) = 2\mathrm{Re}\{\mathbf{A}(\mathbf{r})\mathrm{e}^{-i\omega t}\}$ so that the electric field amplitude reads $\mathbf{E}(\mathbf{r}) = (i\omega/c)\mathbf{A}(\mathbf{r})$, we find the transmitted wave function to reduce to

$$\psi(\mathbf{r},t) = \psi_0(\mathbf{r} - \mathbf{v}t)\mathrm{e}^{i\varphi(\mathbf{R})},$$

where

$$\varphi(\mathbf{R}) = \frac{-1}{\mathcal{M}\omega^2}\int_{-\infty}^{\infty} dz\left[|E_x(\mathbf{r})|^2 + |E_y(\mathbf{r})|^2 + \frac{1}{\gamma^2}|E_z(\mathbf{r})|^2\right] \qquad (2)$$

is an imprinted phase that depends on the transverse coordinates $\mathbf{R} = (x,y)$. Also, we define the scaled mass $\mathcal{M} = m_e\gamma v/c\alpha$ with $\alpha \approx 1/137$ denoting the fine structure constant, and t is taken such that $\psi_0(\mathbf{r} - \mathbf{v}t)$ has already passed the interaction region, which after a change of variables ($z - vt + vt' \to z$) allows us to extend the integral to $z = \infty$.

Description of an OFEM.—We envision an OFEM placed right before the objective lens of an electron microscope [Fig. 1(a)] in a region where the e-beam spans a large diameter ($\gtrsim$100 times the light wavelength). The OFEM could consist of a combination of planar and parabolic

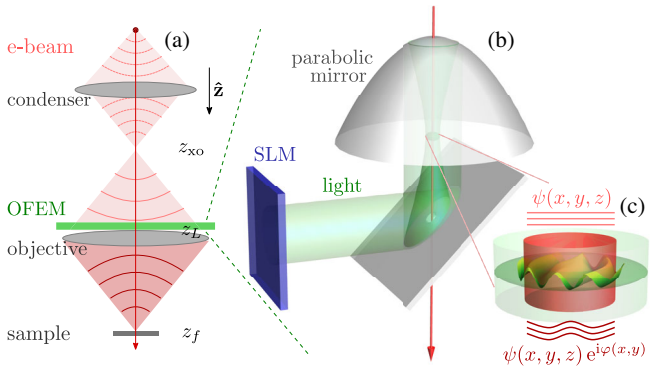

FIG. 1. Optical free-space electron modulator (OFEM). (a) The proposed element is placed in the electron microscope column right before the objective lens. (b) The OFEM incorporates a parabolic mirror that focuses light with a high numerical aperture on a vacuum region that intersects the electron beam. The electric field distribution at the optical focal spot is patterned by using a far-field spatial light modulator (SLM). (c) A phase is imprinted on the electron wave function, whose dependence on transverse coordinates $\mathbf{R}$ is proportional to the field intensity integrated along z.

mirrors with drilled holes that allow the e-beam to pass through the optical focal region [Fig. 1(b)]. The electron is then exposed to intense fields that can be shaped with diffraction-limited lateral resolution through a spatial light modulator and a high numerical aperture in the parabolic mirror. This results in a controlled position-dependent phase, as prescribed by Eq. (2) [Fig. 1(c)]. Considering a monochromatic e-beam and omitting for simplicity an overall $e^{-iE_0t/\hbar}$ time-dependent factor, free propagation of the electron wave function between planes z and z_f is described by

$$\psi(\mathbf{r}_f) = \iint \frac{d^2\mathbf{q}_\perp d^2\mathbf{R}}{(2\pi)^2} e^{i\mathbf{q}_\perp\cdot(\mathbf{R}_f-\mathbf{R})+iq_z(z_f-z)}\psi(\mathbf{r}) \propto \int d^2\mathbf{R} e^{iq_0|\mathbf{R}_f-\mathbf{R}|^2/2(z_f-z)}\psi(\mathbf{r}), \quad (3)$$

where the second line is obtained by performing the $\mathbf{q}_\perp = (q_x, q_y)$ integral in the paraxial approximation (i.e., $q_z = \sqrt{q_0^2 - q_\perp^2} \approx q_0 - q_\perp^2/2q_0$), and we are interested in exploring positions $r_f = (\mathbf{R}_f, z_f)$ near the electron focal point. In a simplified microscope model, we take $z = z_L$ at the entrance of the objective lens where the OFEM is also placed, and the incident electron is a spherical wave $\psi(\mathbf{R}, z_L) \propto e^{iq_0R^2/2(z_L-z_{xo})}$ emanating from the crossover point $\mathbf{r} = (0, 0, z_{xo})$ following the condenser lens. Introducing in Eq. (3) the phase $e^{-iq_0R^2/2f}$ produced by an objective lens with focal distance f and aperture radius R_{max}, we have (see Sec. S3 in the SM [66])

$$\psi(\mathbf{r}_f) \propto \int d^2\vec{\theta} e^{-iq_0\vec{\theta}\cdot\mathbf{R}_f} e^{i\chi(\vec{\theta})+i\varphi(\mathbf{R})} e^{iq_0R^2\Delta/2}, \quad (4)$$

where $\vec{\theta} = \mathbf{R}/(z_f - z_L)$. Also, we define $\Delta = 1/(z_f - z_L) + 1/(z_L - z_{xo}) - 1/f$, the phases χ and φ are produced by aberrations and the OFEM [Eq. (2)], respectively, and the integral is restricted to $\theta < R_{max}/(z_f - z_L)$. In what follows, we study the electron wave function profile $\psi(\mathbf{r}_f)$ as given by Eq. (4) at the focal plane z_f, defined by the condition $\Delta = 0$.

Required light intensity.—From Eq. (2), the imprinted phase shift scales with the light intensity $I_0 = c|E|^2/2\pi$ roughly as $\varphi/I_0 \sim -2\pi L/\mathcal{M}c\omega^2$, where L is the effective length of the light-electron interaction region, which depends on the focusing conditions of the external illumination. For example, for an electron moving along the axis of an optical paraxial vortex beam of azimuthal angular momentum number $m = 1$ and wavelength $\lambda_0 = 2\pi c/\omega$, we have $L \approx 2\lambda_0/\theta_L^2$, where θ_L is the light beam divergence half-angle (see Sec. S5 in the SM [66]). Under these conditions, a phase $\varphi = 2\pi$ is achieved with a light power $\mathcal{P} = 2\mathcal{M}c^2\omega \sim 40$ kW for 60 keV electrons and $\lambda_0 = 500$ nm; this result is independent of θ_L, emphasizing the important role of phase accumulation along a large interaction region in a loosely focused light beam. Perhaps more relevant is the power required to imprint an average phase $\langle\varphi\rangle \sim \pi$ [i.e., $\langle I_0\rangle \sim \mathcal{M}c\omega^2/2L$ from Eq. (2)] over the area πR_{max}^2 of the objective lens aperture; taking $R_{max}/\lambda_0 = 20$, a conservative interaction length $L \sim 1$ μm, and 60 keV electrons, we find a total beam power $\mathcal{P} = \pi R_{max}^2\langle I_0\rangle \sim 40$ MW, which could be distributed in a quasimonochromatic 10 ps pulse to act on sub-ps electron pulses using UTEM technology. We note that the phase scaling $\varphi \propto I_0/(v\gamma\omega^2)$ [see Eq. (2)] leaves some room for improvement by placing the OFEM in low-energy regions of the e-beam to reduce the optical power demand.

Aberration correction.—As an application of lateral phase molding, we explore the conditions needed to compensate for the third-order spherical aberration, which corresponds to [71,72] $\chi(\theta) = C_3q_0\theta^4/4$ in Eq. (4), where C_3 is a length coefficient. Upon examination of the phase profile imprinted by paraxial light vortex beams (see Sec. S4 in the SM [66]), we find that an azimuthal number $m = 3$ produces the required radial dependence $\varphi(R) = -(\pi^5\mathcal{P}/12\mathcal{M}c^2\omega)(\theta_L R/\lambda_0)^4$ under the condition $R \ll \lambda_0/2\pi\theta_L$. For typical microscope parameters $C_3 = f = 1$ mm, 60 keV electrons, $R_{max} = 30$ μm, and $\lambda_0 = 500$ nm, the above condition is satisfied with $\theta_L \ll 0.15°$. Then, the compensation of spherical aberration (i.e., $\varphi = -\chi$) is realized with a beam power $\mathcal{P} = (6\hbar c^2/\pi^4\alpha)C_3q_0^2\lambda_0^3/\theta_L^4(z_f - z_L)^4 \gg 4 \times 10^8$ W, which is attainable using femtosecond laser pulses in UTEMs [41,49,57,58].

Transverse e-beam shaping.—The production of on-demand electron spot profiles involves a two-step process comprising the determination of the necessary phase pattern $\varphi(\mathbf{R})$ and from there the required optical beam parameters that generate that phase. While this is a complex task in general, we can find an approximate

analytical solution for one-dimensional systems, assuming translational invariance along a direction y perpendicular to the electron velocity. We therefore consider an optical beam characterized by an electric field $\mathbf{E}(\mathbf{r}) = E(x,z)\hat{\mathbf{y}}$ and explore the generation of focal electron shapes defined by a wave function $\psi(x,z)$ independent of y. For light propagating along positive z directions, we can write without loss of generality $E(x,z) = \int_{-k_0}^{k_0} (dk_x/2\pi) e^{i(k_x x + k_z z)} \beta_{k_x}$ with $k_z = \sqrt{k_0 - k_x^2}$ and $k_0 = 2\pi/\lambda_0$ in terms of the expansion coefficients β_{k_x}. Inserting this expression into Eq. (2), we find (see Sec. S6 in the SM [66]) $\varphi(x) = \varphi_0 - (1/2\pi\mathcal{M}\omega^2) \int_{-k_0}^{k_0} dk_x e^{2ik_x x} (k_z/|k_x|) \beta_{k_x} \beta^*_{-k_x}$, where φ_0 is a global phase. Given a target profile $\varphi^{\text{target}}(x)$, we can then use the approximation $\beta_{k_x}\beta^*_{-k_x} \approx -2\mathcal{M}\omega^2(|k_x|/k_z) \int dx\, e^{-2ik_x x} \varphi^{\text{target}}(x)$ to generate the needed light beam coefficients. A particular solution is obtained by imposing $\beta_{k_x} = \beta^*_{-k_x}$, which renders β_{k_x} as the square root of the right-hand side in the above expression. For any solution, combining these two integral expressions and dismissing φ_0, we find

$$\varphi(x) = \frac{1}{\pi} \int_{-R_{\max}}^{R_{\max}} dx' \frac{\sin[4\pi(x-x')/\lambda_0]}{x-x'} \varphi^{\text{target}}(x'), \quad (5)$$

which yields a diffraction-limited phase profile.

We explore this strategy in Fig. 2, where the left panels present the OFEM phase and the right ones show the corresponding color-matched wave functions obtained by inserting that phase into Eq. (4) without aberrations ($\chi = 0$) and with the integral over θ_y yielding a trivial overall constant factor. Broken curves in Figs. 2(a), 2(b) and red curves in Figs. 2(c)–2(f) stand for target profiles, whereas the rest of the curves are obtained by accounting for optical diffraction [i.e., by transforming the target phase as prescribed by Eq. (5)]. In-plane OFEM and focal coordinates x and x_f are normalized as explained in the caption, thus defining universal curves for a specific choice of the ratio between the objective aperture radius and the light wavelength $R_{\max}/\lambda_0 = 12.5$. Linear phase profiles [Fig. 2(a)], which are well reproduced by diffraction-limited illumination, give rise to peaked electron wave functions [Fig. 2(b)] centered at positions $x_f = (A/2\pi)\lambda_{e\perp}$ that depend on the slope of the phase $\varphi = Ax/R_{\max} + B$, with the offset value B determining the focal peak phase. The situation is more complicated when aiming to produce two electron peaks, which can be achieved with an intermittent phase profile that combines two different slopes, either without [Figs. 2(c) and 2(d)] or with [Figs. 2(e) and 2(f)] offset to generate symmetric or antisymmetric wave functions, respectively. Light diffraction reduces the contrast of the obtained focal shapes but still tolerates well-defined intensity peaks [Figs. 2(b), 2(d), 2(f), light curves], which become sharper when $R_{\max}/\lambda_0$ is increased (see Fig. S1 in the SM [66]).

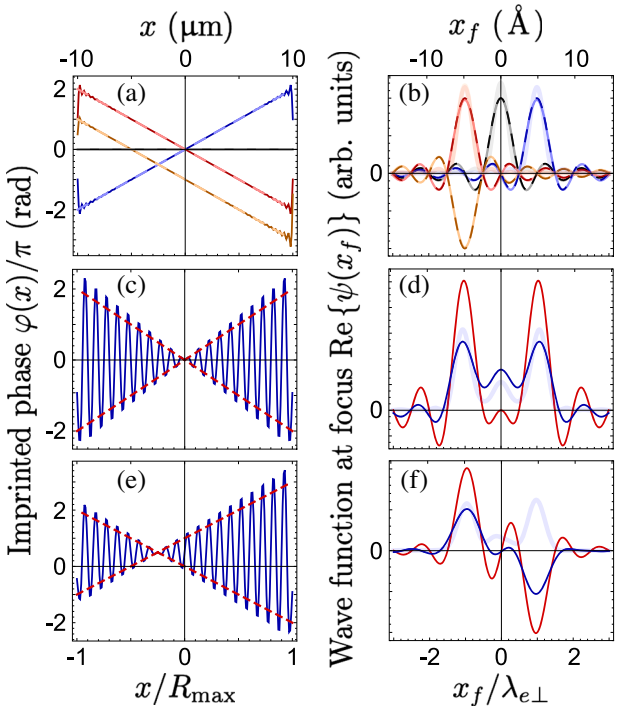

FIG. 2. 1D electron focus shaping. We plot the OFEM-imprinted electron phase [(a),(c),(e)] and the corresponding wave function at the focal plane [(b),(d),(f)]. Dashed curves in (a),(b) and red curves in (c)–(f) correspond to ideal target profiles, while solid curves in (a),(b) and blue curves in (c)–(f) stand for the result obtained by introducing optical diffraction in the OFEM illumination. We consider a linear phase variation (a) leading to single-peak wave functions (b), as well as more complex phase patterns (c),(e) producing symmetric (d) and antisymmetric (f) double-peak wave functions. We take a ratio of the objective-lens semiaperture to the light wavelength $R_{\max}/\lambda_0 = 12.5$. The in-plane OFEM and focal coordinates x and x_f are normalized to $R_{\max}$ and the projected electron Abbe wavelength $\lambda_{e\perp} = \lambda_e/\text{NA}$, respectively, where $\lambda_e = 2\pi/q_0$ is the electron wavelength and $\text{NA} = R_{\max}/(z_f - z_L)$ is the microscope numerical aperture. The electron probability density $|\psi|^2$ is shown as color-matching thick-light curves in (b),(d),(f). Upper horizontal scales correspond to 60 keV electrons, $R_{\max} = 10\ \mu$m, and NA = 0.01.

For actual two-dimensional beams, using the consolidated results of image compression theory [67,68], we can find approximate contour spot profiles by setting the OFEM phase to the argument of the Fourier transform of solid shapes filling those contours. This is illustrated in Fig. 3, where panel (b) represents the phase of the object in (a), while panel (c) is the actual diffraction-limited phase obtained by convoluting (b) with a point spread function $J_1(2\pi R/\lambda_0)/R\lambda_0$ (see Sec. S7 in the SM [66]), which produces a blurred but still discernible electron focal image.

Conclusion.—In brief, shaped optical fields can modulate the electron wave function in free space to produce

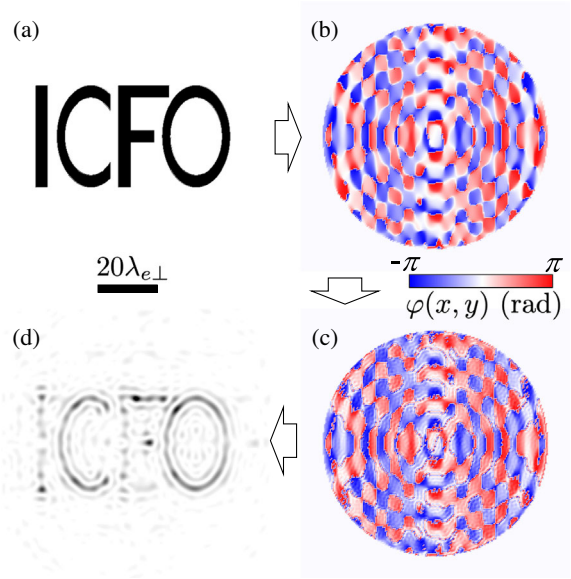

FIG. 3. 2D electron focus shaping. (a) Designated focal shape. (b) Phase of the Fourier transform of (a) (target phase). (c) Diffraction-limited phase to be imprinted by OFEM assuming $R_{\max}/\lambda_0 = 30$. (d) Finally obtained focal profile. The bar shows the scale of (a),(d) in units of $\lambda_{e\perp}$. The phase plots have a radius $R_{\max}$.

on-demand e-beam focal profiles. The required light intensities are reachable using pulsed illumination that is currently available in UTEMs. We have illustrated this idea with simple examples of target optical profiles, but a higher degree of control over the transverse electron wave function should benefit from machine learning techniques [73] for the well-defined problem of finding the optimum light beam angular profile that better fits the desired e-beam spot shape. In combination with spatiotemporal light shaping, the proposed OFEM element should enable the exploration of nanoscale nonlocal correlations in the dynamics of the specimen.

We thank Mathieu Kociak and Ido Kaminer for helpful and enjoyable discussions. This work has been supported in part by European Research Council (Advanced Grant No. 789104eNANO), the European Commission (Horizon 2020 Grants No. FET-Proactive 101017720-EBEAM and No. FET-Open 964591-SMART-electron), the Spanish MINECO (MAT2017-88492-R and SEV2015-0522), the Catalan CERCA Program, and Fundació Privada Cellex.

*Corresponding author.
javier.garciadeabajo@nanophotonics.es

[1] M. Haider, H. Rose, S. Uhlemann, E. Schwan, B. Kabius, and K. Urban, Ultramicroscopy **75**, 53 (1998).
[2] P. E. Batson, N. Dellby, and O. L. Krivanek, Nature (London) **418**, 617 (2002).
[3] P. Hawkes and J. Spence, *Springer Handbook of Microscopy* (Springer Nature Switzerland AG, 2019).
[4] P. D. Nellist, M. F. Chisholm, N. Dellby, O. L. Krivanek, M. F. Murfitt, Z. S. Szilagyi, A. R. Lupini, A. Borisevich, W. H. Sides, Jr., and S. J. Pennycook, Science **305**, 1741 (2004).
[5] D. A. Muller, L. Fitting Kourkoutis, M. Murfitt, J. H. Song, H. Y. Hwang, J. Silcox, N. Dellby, and O. L. Krivanek, Science **319**, 1073 (2008).
[6] O. L. Krivanek, T. C. Lovejoy, N. Dellby, T. Aoki, R. W. Carpenter, P. Rez, E. Soignard, J. Zhu, P. E. Batson, M. J. Lagos *et al.*, Nature (London) **514**, 209 (2014).
[7] M. J. Lagos, A. Trügler, U. Hohenester, and P. E. Batson, Nature (London) **543**, 529 (2017).
[8] F. S. Hage, R. J. Nicholls, J. R. Yates, D. G. McCulloch, T. C. Lovejoy, N. Dellby, O. L. Krivanek, K. Refson, and Q. M. Ramasse, Sci. Adv. **4**, eaar7495 (2018).
[9] F. S. Hage, D. M. Kepaptsoglou, Q. M. Ramasse, and L. J. Allen, Phys. Rev. Lett. **122**, 016103 (2019).
[10] J. A. Hachtel, J. Huang, I. Popovs, S. Jansone-Popova, J. K. Keum, J. Jakowski, T. C. Lovejoy, N. Dellby, O. L. Krivanek, and J. C. Idrobo, Science **363**, 525 (2019).
[11] G. Möllenstedt and H. Düker, Z. Phys. **145**, 377 (1956).
[12] J. Verbeeck, G. Bertoni, and P. Schattschneider, Ultramicroscopy **108**, 263 (2008).
[13] C. Bäuerle, D. C. Glattli, T. Meunier, F. Portier, P. Roche, P. Roulleau, S. Takada, and X. Waintal, Rep. Prog. Phys. **81**, 056503 (2018).
[14] G. Guzzinati, A. Beche, H. Lourenco-Martins, J. Martin, M. Kociak, and J. Verbeeck, Nat. Commun. **8**, 14999 (2017).
[15] A. Béché, R. Van Boxem, G. Van Tendeloo, and J. Verbeeck, Nat. Phys. **10**, 26 (2014).
[16] J. Verbeeck, A. Béché, K. Müller-Caspary, G. Guzzinati, M. A. Luong, and M. D. Hertog, Ultramicroscopy **190**, 58 (2018).
[17] J. Verbeeck, H. Tian, and P. Schattschneider, Nature (London) **467**, 301 (2010).
[18] B. J. McMorran, A. Agrawal, I. M. Anderson, A. A. Herzing, H. J. Lezec, J. J. McClelland, and J. Unguris, Science **331**, 192 (2011).
[19] R. Shiloh, Y. Lereah, Y. Lilach, and A. Arie, Ultramicroscopy **144**, 26 (2014).
[20] V. Grillo, A. H. Tavabi, E. Yucelen, P.-H. Lu, F. Venturi, H. Larocque, L. Jin, A. Savenko, G. C. Gazzadi, R. Balboni *et al.*, Opt. Express **25**, 21851 (2017).
[21] R. Shiloh, R. Remez, P.-H. Lu, L. Jin, Y. Lereah, A. H. Tavabi, R. E. Dunin-Borkowski, and A. Arie, Ultramicroscopy **189**, 46 (2018).
[22] P. L. Kapitza and P. A. M. Dirac, Proc. Cambridge Philos. Soc. **29**, 297 (1933).
[23] D. L. Freimund, K. Aflatooni, and H. Batelaan, Nature (London) **413**, 142 (2001).
[24] D. L. Freimund and H. Batelaan, Phys. Rev. Lett. **89**, 283602 (2002).
[25] H. Batelaan, Rev. Mod. Phys. **79**, 929 (2007).
[26] F. J. García de Abajo, Rev. Mod. Phys. **82**, 209 (2010).
[27] M. Kozák, N. Schönenberger, and P. Hommelhoff, Phys. Rev. Lett. **120**, 103203 (2018).
[28] M. Kozák, Phys. Rev. Lett. **123**, 203202 (2019).

[29] D. S. Black, U. Niedermayer, Y. Miao, Z. Zhao, O. Solgaard, R. L. Byer, and K. J. Leedle, Phys. Rev. Lett. **123**, 264802 (2019).

[30] N. Schönenberger, A. Mittelbach, P. Yousefi, J. McNeur, U. Niedermayer, and P. Hommelhoff, Phys. Rev. Lett. **123**, 264803 (2019).

[31] A. Howie, Inst. Phys. Conf. Ser. **161**, 311 (1999).

[32] F. J. García de Abajo and M. Kociak, New J. Phys. **10**, 073035 (2008).

[33] A. Howie, Microsc. Microanal. **15**, 314 (2009).

[34] E. Pomarico, I. Madan, G. Berruto, G. M. Vanacore, K. Wang, I. Kaminer, F. J. García de Abajo, and F. Carbone, ACS Photonics **5**, 759 (2018).

[35] B. Barwick, D. J. Flannigan, and A. H. Zewail, Nature (London) **462**, 902 (2009).

[36] F. J. García de Abajo, A. Asenjo-Garcia, and M. Kociak, Nano Lett. **10**, 1859 (2010).

[37] S. T. Park, M. Lin, and A. H. Zewail, New J. Phys. **12**, 123028 (2010).

[38] S. T. Park and A. H. Zewail, J. Phys. Chem. A **116**, 11128 (2012).

[39] F. O. Kirchner, A. Gliserin, F. Krausz, and P. Baum, Nat. Photonics **8**, 52 (2014).

[40] L. Piazza, T. T. A. Lummen, E. Quiñonez, Y. Murooka, B. Reed, B. Barwick, and F. Carbone, Nat. Commun. **6**, 6407 (2015).

[41] A. Feist, K. E. Echternkamp, J. Schauss, S. V. Yalunin, S. Schäfer, and C. Ropers, Nature (London) **521**, 200 (2015).

[42] T. T. A. Lummen, R. J. Lamb, G. Berruto, T. LaGrange, L. D. Negro, F. J. García de Abajo, D. McGrouther, B. Barwick, and F. Carbone, Nat. Commun. **7**, 13156 (2016).

[43] K. E. Echternkamp, A. Feist, S. Schäfer, and C. Ropers, Nat. Phys. **12**, 1000 (2016).

[44] A. Ryabov and P. Baum, Science **353**, 374 (2016).

[45] G. M. Vanacore, A. W. P. Fitzpatrick, and A. H. Zewail, Nano Today **11**, 228 (2016).

[46] M. Kozák, J. McNeur, K. J. Leedle, H. Deng, N. Schönenberger, A. Ruehl, I. Hartl, J. S. Harris, R. L. Byer, and P. Hommelhoff, Nat. Commun. **8**, 14342 (2017).

[47] A. Feist, N. Bach, T. D. N. Rubiano da Silva, M. Mäller, K. E. Priebe, T. Domräse, J. G. Gatzmann, S. Rost, J. Schauss, S. Strauch *et al.*, Ultramicroscopy **176**, 63 (2017).

[48] K. E. Priebe, C. Rathje, S. V. Yalunin, T. Hohage, A. Feist, S. Schäfer, and C. Ropers, Nat. Photonics **11**, 793 (2017).

[49] G. M. Vanacore, I. Madan, G. Berruto, K. Wang, E. Pomarico, R. J. Lamb, D. McGrouther, I. Kaminer, B. Barwick, F. J. García de Abajo *et al.*, Nat. Commun. **9**, 2694 (2018).

[50] Y. Morimoto and P. Baum, Phys. Rev. A **97**, 033815 (2018).

[51] Y. Morimoto and P. Baum, Nat. Phys. **14**, 252 (2018).

[52] P. Das, J. D. Blazit, M. Tencé, L. F. Zagonel, Y. Auad, Y. H. Lee, X. Y. Ling, A. Losquin, O. S. C. Colliex, F. J. García de Abajo *et al.*, Ultramicroscopy **203**, 44 (2019).

[53] G. M. Vanacore, G. Berruto, I. Madan, E. Pomarico, P. Biagioni, R. J. Lamb, D. McGrouther, O. Reinhardt, I. Kaminer, B. Barwick *et al.*, Nat. Mater. **18**, 573 (2019).

[54] O. Kfir, Phys. Rev. Lett. **123**, 103602 (2019).

[55] V. Di Giulio, M. Kociak, and F. J. García de Abajo, Optica **6**, 1524 (2019).

[56] N. Talebi, Phys. Rev. Lett. **125**, 080401 (2020).

[57] O. Kfir, H. Lourenço-Martins, G. Storeck, M. Sivis, T. R. Harvey, T. J. Kippenberg, A. Feist, and C. Ropers, Nature (London) **582**, 46 (2020).

[58] K. Wang, R. Dahan, M. Shentcis, Y. Kauffmann, A. B. Hayun, O. Reinhardt, S. Tsesses, and I. Kaminer, Nature (London) **582**, 50 (2020).

[59] F. J. García de Abajo, B. Barwick, and F. Carbone, Phys. Rev. B **94**, 041404(R) (2016).

[60] A. Feist, S. V. Yalunin, S. Schäfer, and C. Ropers, Phys. Rev. Research **2**, 043227 (2020).

[61] W. Cai, O. Reinhardt, I. Kaminer, and F. J. García de Abajo, Phys. Rev. B **98**, 045424 (2018).

[62] A. Konečná and F. J. García de Abajo, Phys. Rev. Lett. **125**, 030801 (2020).

[63] H. Müller, J. Jin, R. Danev, J. Spence, H. Padmore, and R. M. Glaeser, New J. Phys. **12**, 073011 (2010).

[64] O. Schwartz, J. J. Axelrod, S. L. Campbell, C. Turnbaugh, R. M. Glaeser, and H. Müller, Nat. Methods **16**, 1016 (2019).

[65] J. J. Axelrod, S. L. Campbell, O. Schwartz, C. Turnbaugh, R. M. Glaeser, and H. Müller, Phys. Rev. Lett. **124**, 174801 (2020).

[66] See Supplemental Material, which includes Refs. [38,55, 67–70], at http://link.aps.org/supplemental/10.1103/PhysRevLett.126.123901 for additional results, including derivations of Eqs. (1), (4), and (5).

[67] M. Hayes, J. Lim, and A. Oppenheim, IEEE Trans. Acoustics Speech Signal Process. **28**, 672 (1980).

[68] D. Aiger and H. Talbot, in *2010 IEEE Computer Society Conference on Computer Vision and Pattern Recognition* (IEEE, San Francisco, 2010), pp. 295–302.

[69] A. Messiah, *Quantum Mechanics* (North-Holland, New York, 1966).

[70] W. H. Press, S. A. Teukolsky, W. T. Vetterling, and B. P. Flannery, *Numerical Recipes* (Cambridge University Press, New York, 1992).

[71] L. J. Allen, M. P. Oxley, and D. Paganin, Phys. Rev. Lett. **87**, 123902 (2001).

[72] D. M. Paganin, T. C. Petersen, and M. A. Beltran, Phys. Rev. A **97**, 023835 (2018).

[73] S. R. Spurgeon, C. Ophus, L. Jones, A. Petford-Long, S. V. Kalinin, M. J. Olszta, R. E. Dunin-Borkowski, N. Salmon, K. Hattar, W.-C. D. Yang *et al.*, Nat. Mater. **20**, 274 (2020).